Journal of the Iranian Chemical Society
https://doi.org/10.1007/s13738-019-01788-y

ORIGINAL PAPER

# Organic base grafted on magnetic nanoparticles as a recoverable catalyst for the green synthesis of hydropyridine rings

**Mohammad Ali Bodaghifard**[1,2]

Received: 9 August 2018 / Accepted: 24 September 2019

## Abstract

Synthesis of 4-aminiquinaldine grafted on silica-coated nano-$Fe_3O_4$ particles (MNPs-AQ) and their performance as a retrievable heterogeneous basic catalyst are disclosed. The catalytic performance of this novel material was studied for the green synthesis of substituted 1,4-dihydropyridine and polyhydroquinoline derivatives via one-pot multicomponent reactions. Eco-friendly method, high yield and purity of the desired products, and short reaction time along with the ease of the work-up procedure outline the advantages of these new methodologies over the earlier ones. The surface and magnetic properties of the core/shell hybrid nanoparticles were characterized via TEM, SEM, XRD, EDS, and FT-IR analysis techniques. This nanocatalyst is recyclable without any deterioration in its catalytic activity.

**Keywords** 1,4-Dihydropyridines · Polyhydroquinoline · Green chemistry · Hybrid nanoparticles

## Introduction

1,4-Dihydropyridines (1,4-DHPs) are valuable heterocyclic compounds in view of pharmaceuticals and drugs development [1, 2]. 1,4-DHPs possess a wide range of biological activities such as anti-atherosclerotic [3], vasodilator [4], anti-diabetic [5], geroprotective and hepatoprotective [6], and group of calcium modulators for the treatment of cardiovascular diseases [7]. Realizing the importance of 1,4-dihydropyridine derivatives, increasing interest by 1,4-DHPs as synthetic targets is ongoing. Hantzsch reaction is commonly used for the preparation of 1,4-DHPs [8]. This method involves cyclocondensation of an aldehyde, 1,3-dicarbonyl compounds or CH-acids, and ammonia (or primary amine) either in acetic acid or in refluxing ethanol for long reaction times which typically leads to low yields [9]. In recent years, several modified synthesis methods to access 1,4-DHPs have been developed [10] like $FeF_3$ [11], organocatalysts [12], microwave assisted [13], cellulose sulfuric acid [14], nano-ZnO [15], CAN [16], $I_2$ [17, 18], metal triflates [19], heteropolyacid catalyst [20], ionic liquids [21, 22], 3,4,5-trifluorobenzeneboronic acid [23], iodotrimethylsilane (TMSI) generated in situ in $CH_3CN$ [24], thiamine hydrochloride [25], bismuth nitrate [26], triphenylphosphine [27], and sulfated polyborate [28]. Although some reactions are satisfactory in terms of yield, the use of high temperatures, expensive metal precursors, catalysts that are harmful to the environment, and long reaction times are some drawbacks of these methods.

Organic–inorganic hybrid materials are of great interest as heterogeneous catalysts in organic synthesis, due to the functional diversity merged with thermal and mechanical stability of inorganic solids [29–31]. Their large surface area per unit volume makes them interesting in the heterogeneous catalysis area; Heterogeneous catalysis in the nano-scale takes advantage of a high exposure of the active species leading to a higher efficiency of the catalyst [32, 33]. Nevertheless, the application of heterogeneous nano-catalysts is usually limited by the inevitable loss of catalyst during the tedious separation processes, i.e., filtration or centrifugation. In this vein, easily separable magnetic nanoparticles (MNPs), e.g., $Fe_3O_4$, have demonstrated high stability, easy synthesis, and functionalization alongside with high

---

**Electronic supplementary material** The online version of this article (https://doi.org/10.1007/s13738-019-01788-y) contains supplementary material, which is available to authorized users.

✉ Mohammad Ali Bodaghifard
mbodaghi2007@yahoo.com; m-bodaghifard@araku.ac.ir

[1] Department of Chemistry, Faculty of Science, Arak University, Arak 38156-88138, Iran

[2] Institute of Nanosciences and Nanotechnology, Arak University, Arak, Iran

surface area, low toxicity, and cost. These superb properties set magnetic nanoparticles as a target for extensive investigation as inorganic supports in the synthesis of semi-heterogeneous catalysts [34–38]. These metallic nanoparticles can be coated with silica shell to introduce numerous surface Si–OH groups for further modification and higher chemical and colloidal stability since the magnetically agglomeration will be diminished [29–31, 39, 40].

As part of our continuous effort to develop efficient heterogeneous magnetic nano-catalysts and green organic reactions [29–31, 41–43], and for the above reasons, herein we describe the synthesis and characterization of 4-aminoquinaldine-grafted magnetite nanoparticles (MNPs-AQ) to give access to biologically interesting 1,4-dihydropyridines as a new eco-friendly method (Scheme 1). This newly design catalyst fulfilled our endeavor toward a heterogeneous system with a green synthetic aspects by avoiding the use of hazardous conditions for accessing target heterocyclic compounds.

## Results and discussion

### Preparation and characterization of the catalyst

The magnetic nanoparticle supported 4-aminoquinaldine catalyst (MNPs-AQ) was prepared via sequential reactions as shown in Scheme 2. Magnetite ($Fe_3O_4$) nanoparticles were prepared easily via the chemical co-precipitation of $Fe^{2+}$ and $Fe^{3+}$ ions in basic solution [29–31, 44]. These were subsequently coated with silica layer ($Fe_3O_4$@$SiO_2$) through the well-known Stober method [45]. The $Fe_3O_4$@$SiO_2$ core–shell structures were treated with 3-chloropropyltrimethoxysilane (CPTMS), which can bind covalently to the free-OH groups at the particles surface and afforded the $Fe_3O_4$@$SiO_2$-PrCl. 4-aminoquinaldine grafted on silica-coated magnetite nanoparticles (MNPs-AQ) prepared with the reaction of the 3-chloropropyl-functionalized silica-coated magnetic nanoparticles ($Fe_3O_4$@$SiO_2$-PrCl) and 4-aminoquinaldine.

The FT-IR spectrum of $Fe_3O_4$, $Fe_3O_4$@$SiO_2$, $Fe_3O_4$@$SiO_2$-PrCl, and $Fe_3O_4$@$SiO_2$-AQ nanoparticles in the wavenumber range of 4000–400 $cm^{-1}$ is shown in Fig. 1. The magnetic $Fe_3O_4$ nanoparticles' FT-IR spectra (Fig. 1a) showed the characteristic Fe–O absorption near 578 $cm^{-1}$. FT-IR spectrum of $Fe_3O_4$@$SiO_2$ displays bands at about 1087 (asymmetric stretching), 955 (symmetric stretching), 781 (in plane bending), and 461 $cm^{-1}$ (rocking mode) of the Si–O–Si group and confirm the formation of $SiO_2$ shell. The broad peaks in the range 3200–3500 $cm^{-1}$ (Si–OH stretching vibration mode) and the weak peak at 1639 $cm^{-1}$ (twisting vibration mode of H–O–H adsorbed in the silica shell) are obvious in the spectrum. The weak aliphatic vibrations at

**Scheme 1** Synthesis of 1,4-dihydropyridine derivatives using novel MNPs-AQ as catalyst

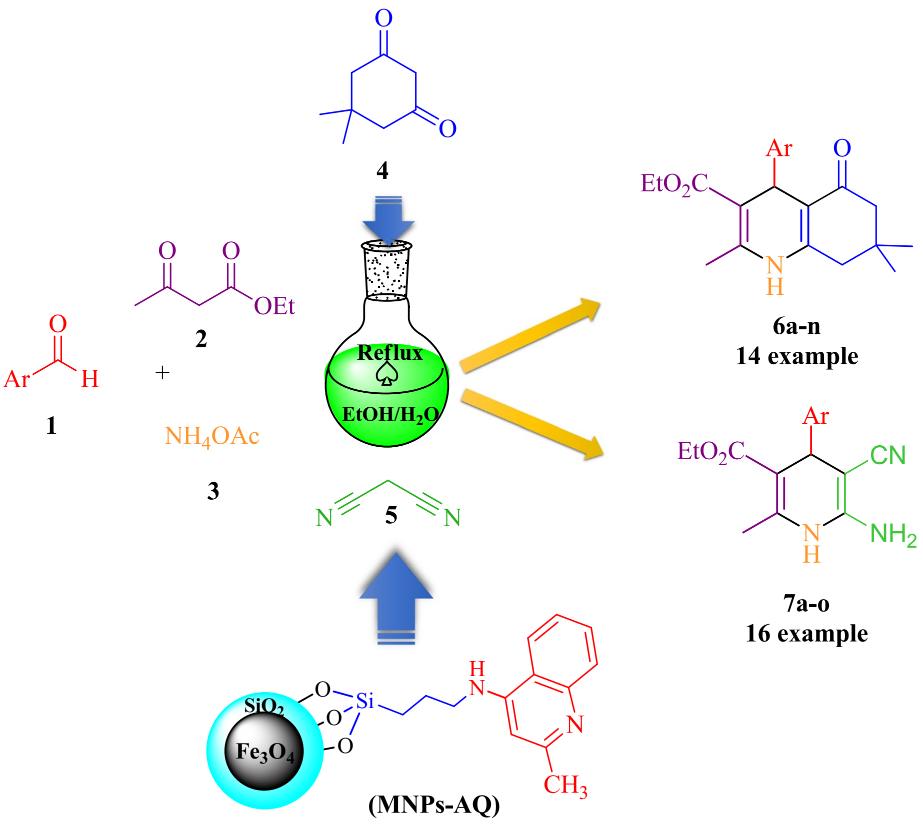

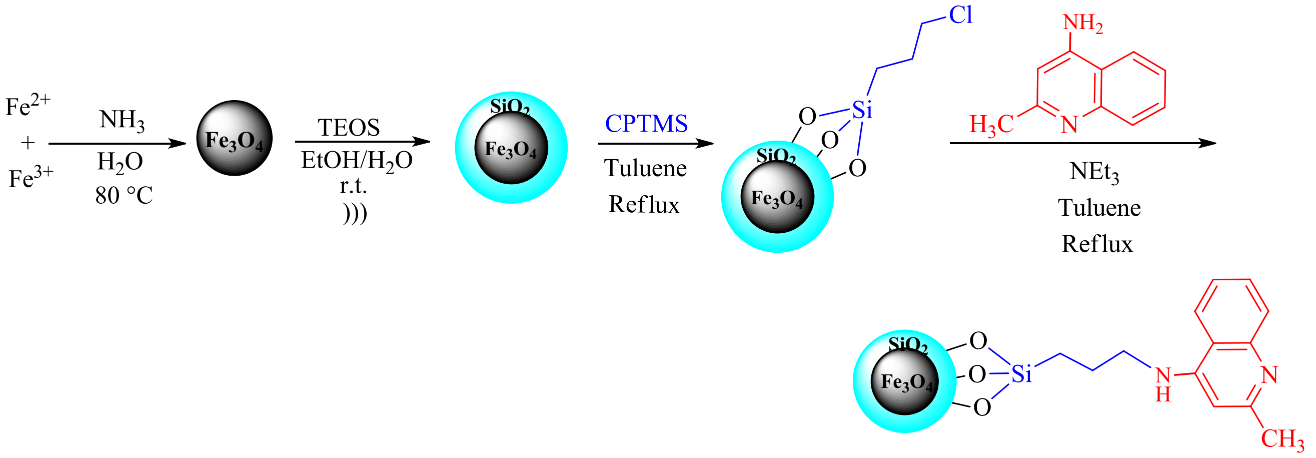

**Scheme 2** Preparation of 4-aminoquinaldine grafted on silica-coated nano-$Fe_3O_4$ particles

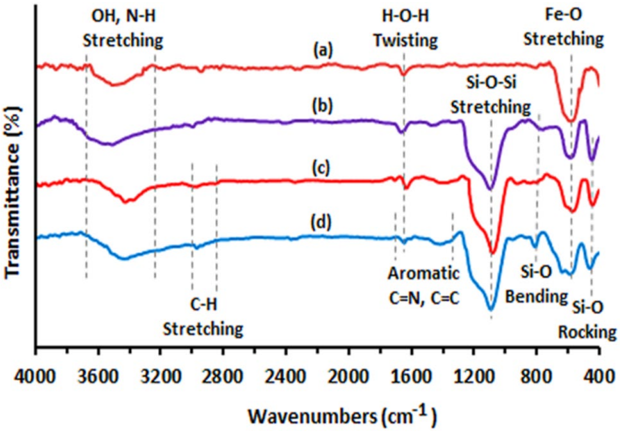

**Fig. 1** Comparative FT-IR spectra for (a) $Fe_3O_4$, (b) $Fe_3O_4@SiO_2$, (c) $Fe_3O_4@SiO_2$-PrCl, (d) $Fe_3O_4@SiO_2$-AQ

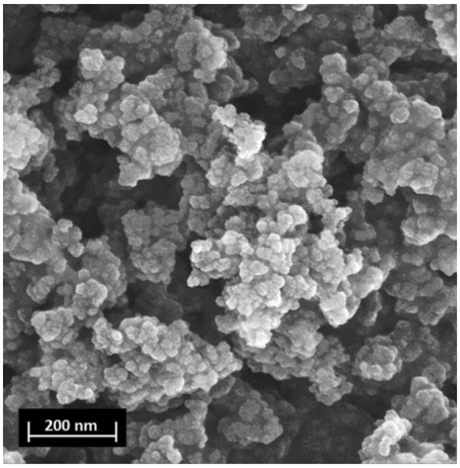

**Fig. 2** The FE-SEM images of MNPs–AQ nanoparticles

2933 and 2940 $cm^{-1}$ (Fig. 1c, d) are related to C–H symmetric and asymmetric stretching and confirmed the presence of the attached alkyl groups. The peaks correspond to C=N and C=C in heterocyclic rings are appeared at 1400–1600 $cm^{-1}$ (Fig. 1d). N–H bending appeared at 1647 $cm^{-1}$ (Fig. 1d) [46]. Therefore, the above results prove that the functional groups were successfully grafted onto the surface of the magnetic $Fe_3O_4@SiO_2$ nanoparticles.

The nanoparticle size and morphology of MNPs-AQ catalyst were surveyed by field emission scanning electron microscopy (FE-SEM) (Fig. 2). As can be seen from Fig. 2, MNPs-AQ particles have a mean diameter of 25–35 nm and a nearly spherical shape.

The energy dispersive X-ray spectroscopy (EDS) results, obtained from SEM analysis of MNPs-AQ, are shown in Fig. 3, and clearly show the presence of Si, O, N, and Fe signals in MNPs-AQ, and the higher intensity of the Si peak

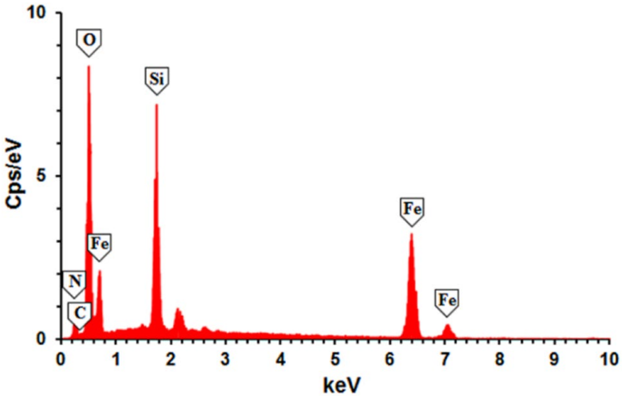

**Fig. 3** The EDS spectrum of MNPs-AQ nanoparticles

compared with the Fe peaks indicates that the $Fe_3O_4$ nanoparticles were trapped by $SiO_2$ layer. According to the above analysis, it can be concluded that the MNPs-AQ have been successfully synthesized.

The presence and degree of crystallinity of magnetic $Fe_3O_4$ and the MNPs-AQ catalyst was considered from XRD measurements (Fig. 4). The same peaks were observed in the both of the magnetic $Fe_3O_4$ and MNPs-AQ XRD patterns, indicating retention of the crystalline spinel ferrite core structure during the silica-coating and functionalization processes. The XRD data of the synthesized magnetic nanoparticles show diffraction peaks at $2\theta = 30.4°$,35.8°, 43.3°, 53.9°, 57.3°, 63°, and 74.5° which can be assigned to the (220), (311), (400), (422), (511), (440), and (533) planes of $Fe_3O_4$, respectively, indicating that the $Fe_3O_4$ particles in the nanoparticles were pure $Fe_3O_4$ with a cubic spinel structure; these matches well with the standard $Fe_3O_4$ sample (JCPDS Card No. 85-1436). The broad peak from $2\theta = 20°$ to 27° (Fig. 5b) is consistent with an amorphous silica phase in the shell of the silica-coated $Fe_3O_4$ nanoparticles ($Fe_3O_4$@$SiO_2$) [47]. The (311) XRD peak was used to estimate the average crystallite size of the magnetic nanoparticles by Scherrer's equation ($D = 0.9\lambda/\beta \cos \theta$), where $D$ is the average crystalline size, $\lambda$ is the X-ray wavelength (0.154 nm), $\beta$ denotes the full width in radians subtended by the half maximum intensity width of the (311) powder peak, and $\theta$ corresponds to the Bragg angle of the (311) peak in degrees [48]. From the width of the peak at $2\theta = 35.7$ (311), the crystallite size of the magnetic nanoparticle is calculated to be 20.1 nm using Scherrer's equation, which is in near range of the size determined by FE-SEM analysis (Fig. 2).

The stability of the MNPs-AQ catalyst was determined by thermogravimetric analysis (TGA) and derivative thermogravimetry (DTG) (Fig. 5). The magnetic catalyst shows two-step weight loss steps over the temperature range of TG analysis (Fig. 6). The first stage, including a low amount of weight loss (2%) at $T < 250$ °C, is due to the removal of physically adsorbed solvent and surface hydroxyl groups, the second stage at about 250 °C to nearly 620 °C is attributed to the decomposition of the organic moiety in the nanocomposite. Therefore, the weight loss between 250 and 620 °C gives the organic grafting ratios of the magnetic catalyst. The grafted organic moiety on the magnetic $Fe_3O_4$@$SiO_2$ nanoparticles was approximately 22 wt%. In accordance with this mass loss, it was calculated that 0.8 mmol of 4-AQ was loaded on 1 g of MNPs-AQ catalyst and are accessible for catalytic reaction processes. Therefore, the MNPs-AQ is stable around or below 250 °C.

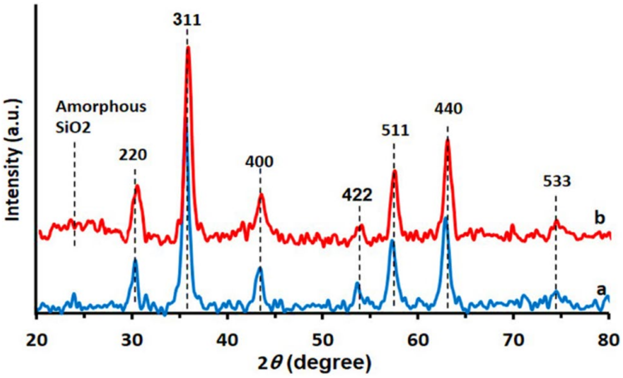

**Fig. 4** XRD diffraction pattern of $Fe_3O_4$ MNPs (**a**), and MNPs-AQ (**b**)

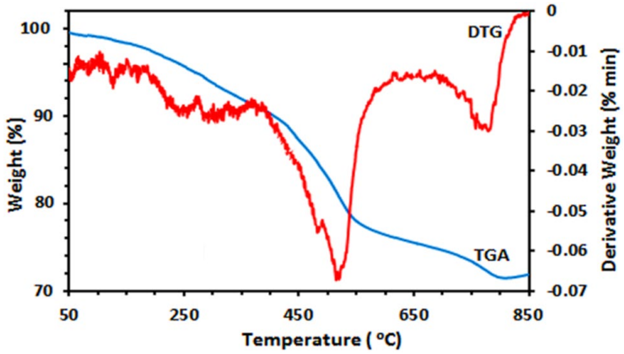

**Fig. 5** TG-DTG analyses for MNPs-AQ nanoparticles

The magnetic properties of nanoparticles were measured by VSM (magnetic vibration measurement). Figure 6 illustrates the magnetic nanoparticle curve at the room temperature, which contains the magnetization ($M$) against magnetic field ($H$) (hysteresis loops) of $Fe_3O_4$, MNPs-AQ. The hysteresis curve provides important information about magnetic properties such as the saturation magnetization ($M_s$), remanent magnetization ($M_r$), and coercivity ($H_c$). It is obvious that by increasing the magnetic field, the magnetization increases rapidly and it fixed in the 10,000 Os field and the sample is saturated completely. As shown in the Fig. 6, the $M_s$ of MNPs-AQ is altered from 64 to 42 emu $g^{-1}$ because the silica shell is formed around the $Fe_3O_4$. The hysteresis

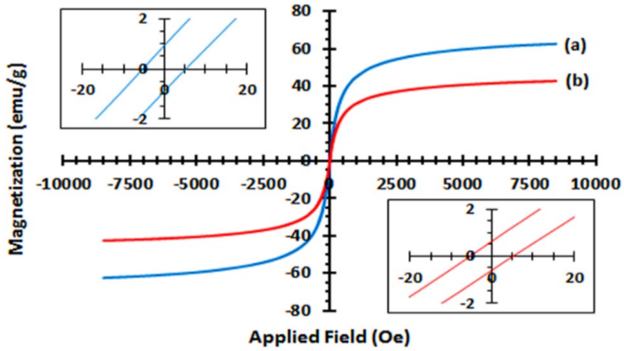

**Fig. 6** Magnetic hysteresis loops of **a** $Fe_3O_4$ MNPs and **b** MNPs-AQ

curve indicates the super paramagnetic properties for $Fe_3O_4$, MNPs-AQ which the $M_r$ and $H_c$ are near the zero [48, 49].

After the characterization of the MNPs-AQ hybrid nanomaterial, its catalytic activity was evaluated for the synthesis of 1,4-dihydropyridine derivatives (Scheme 1). An important feature of these nano-catalysts is simple separation of them using an external magnet, thereby removing the necessity for filtration or centrifugation. In order to optimize the reaction conditions and obtain the best catalytic activity, the reaction of benzaldehyde (1 mmol), malononitrile, ethylacetoacetate, and ammonium acetate was used as a model and was conducted under different reaction parameters (Table 1). As shown in Table 1 (entry 7), the best result was found in $H_2O$/EtOH (1:1) at reflux condition using 30 mg of the catalyst. Moreover, the catalyst is essential and in the absence of the catalyst, only 17% of the corresponding 1,4-dihydropyridine was produced even after prolonged reaction times (Table 1, entry 13). The efficiencies of $Fe_3O_4$, $Fe_3O_4$@$SiO_2$ and MNPs-PrCl and MNPs-AQ as the catalyst toward the model reaction were compared and the results are depicted in Table 1. It was observed that the MNPs-AQ was more efficient than the other ones (entries 7 and 14–16).

In order to determine the generality and efficacy of the catalyst, different kinds of aromatic aldehyde carrying either electron-donating or electron-withdrawing groups were reacted under the optimized reaction condition (Scheme 1, Table 2). All reactions proceeded efficiently in the presence of catalytic amounts of MNPs-AQ in reflux condition, and the desired products were obtained in good to excellent yields (83–96%) at relatively short reaction times, without formation of side products.

A plausible mechanism for the formation of 1,4-dihydropyridine derivatives catalyzed by MNPs-AQ is shown in Scheme 3. The MNPs-AQ catalyst deprotonates the malononitrile and facilitates the Knoevenagel condensation to produce the arylidene malononitrile intermediate. The Michael addition of activated ethylacetoacetate in the presence of MNPs-AQ to arylidene malononitrile resulted in the intermediate. The condensation of intermediate with ammonium acetate and subsequent tautomerization produce the corresponding 1,4-dihydropyridine.

The results of this study are compared with some existing methods for the preparation of 1,4-dihydropyridine and polyhydroquinoline derivatives in the literature. The results of these catalysts in the condensation reaction of benzaldehyde, ethylacetoacetate, dimedone, and ammonium acetate under optimized conditions have been indicated in Table 3. As can be seen, the catalytic system reported in this paper has benefits in terms of simple conditions, short reaction times, and excellent yields and is superior to many other methods.

**Table 1** Optimization of reaction conditions for preparation of 1,4-dihydropyridine derivatives

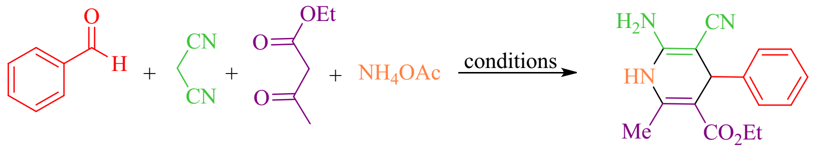

| No. | Catalyst (mg) | Solvent | Temp. (°C) | Time (min) | Yield (%)[a] |
|---|---|---|---|---|---|
| 1 | MNPs-AQ (20) | THF | Reflux | 45 | 63 |
| 2 | MNPs-AQ (20) | $CH_3CN$ | Reflux | 45 | 53 |
| 3 | MNPs-AQ (20) | $CH_2Cl_2$ | Reflux | 45 | 41 |
| 4 | MNPs-AQ (20) | EtOH | Reflux | 30 | 81 |
| 5 | MNPs-AQ (30) | EtOH | Reflux | 30 | 93 |
| 6 | MNPs-AQ (20) | $H_2O$ | Reflux | 45 | 47 |
| 7 | MNPs-AQ (30) | EtOH:$H_2O$ | Reflux | 30 | 95 |
| 8 | MNPs-AQ (50) | EtOH:$H_2O$ | Reflux | 30 | 94 |
| 9 | MNPs-AQ (30) | EtOH:$H_2O$ | 60 | 30 | 76 |
| 10 | MNPs-AQ (30) | EtOH:$H_2O$ | 40 | 30 | 56 |
| 11 | MNPs-AQ (30) | EtOH:$H_2O$ | r.t. | 30 | 43 |
| 12 | MNPs-AQ (30) | – | 100 | 30 | 87 |
| 13 | – | EtOH:$H_2O$ | Reflux | 90 | 17 |
| 14 | $Fe_3O_4$ (30) | EtOH:$H_2O$ | Reflux | 30 | 49 |
| 15 | $Fe_3O_4$@$SiO_2$ (30) | EtOH:$H_2O$ | Reflux | 30 | 48 |

[a] Isolated yields

**Table 2** Multicomponent one-pot synthesis of 1,4-dihydropyridine derivatives

| Product | Ar | Time (min) | Yield (%)[a] | MP (°C)[b] | |
|---|---|---|---|---|---|
| | | | | Found | Reported |
| **6a** | $C_6H_5$ | 30 | 96 | 204–205 | 202–204 [16] |
| **6b** | $3\text{-}NO_2–C_6H_4$ | 35 | 93 | 179–181 | 178–179 [17] |
| **6c** | $4\text{-}NO_2–C_6H_4$ | 30 | 95 | 240–242 | 243–244 [17] |
| **6d** | $4\text{-}Cl–C_6H_4$ | 30 | 93 | 242–244 | 245–246 [17] |
| **6e** | $4\text{-}Br–C_6H_4$ | 35 | 93 | 252–253 | 253–255 [16] |
| **6f** | $4\text{-}CH_3–C_6H_4$ | 35 | 92 | 260–262 | 260–261 [16] |
| **6g** | $4\text{-}OH–C_6H_4$ | 40 | 93 | 232–233 | 230–231 [17] |
| **6h** | $4\text{-}OMe–C_6H_4$ | 40 | 90 | 253–255 | 255–257 [17] |
| **6i** | $4\text{-}N(Me)_2–C_6H_4$ | 35 | 92 | 259–261 | 262–263 [17] |
| **6j** | $3\text{-}OH–C_6H_4$ | 35 | 91 | 230–232 | 236–238 [16] |
| **6k** | $2\text{-}Cl–C_6H_4$ | 30 | 90 | 204–205 | 207–208 [17] |
| **6l** | $2,4\text{-}Cl_2–C_6H_3$ | 30 | 95 | 240–241 | 241–243 [15] |
| **6m** | $3,4\text{-}(OCH_3)–C_6H_3$ | 35 | 91 | 202–203 | 198–199 [17] |
| **6n** | $C_6H_5–CH{=}CH\text{-}$ | 35 | 87 | 199–201 | 204–206 [16] |
| **7a** | $C_6H_5$ | 30 | 95 | 185–187 | 188–190 [50] |
| **7b** | $4\text{-}Cl–C_6H_4$ | 30 | 96 | 217–219 | 221–223 [50] |
| **7c** | $4\text{-}Br–C_6H_4$ | 35 | 93 | 201–203 | 197–199 [51] |
| **7d** | $4\text{-}F–C_6H_4$ | 30 | 90 | 229–230 | 223–225 [52] |
| **7e** | $2\text{-}NO_2–C_6H_4$ | 35 | 91 | 126–128 | 123–125 [52] |
| **7f** | $3\text{-}NO_2–C_6H_4$ | 30 | 93 | 161–163 | 158–159 [53] |
| **7g** | $4\text{-}NO_2–C_6H_4$ | 30 | 95 | 177–178 | 173–175 [50] |
| **7h** | $4\text{-}OMe–C_6H_4$ | 40 | 90 | 191–193 | 188–190 [52] |
| **7i** | $3\text{-}OMe–C_6H_4$ | 35 | 87 | 187–188 | 192–194 [51] |
| **7j** | $2\text{-}OMe–C_6H_4$ | 35 | 90 | 207–209 | 209–211 [52] |
| **7k** | $3,4\text{-}(OCH_3)–C_6H_3$ | 30 | 90 | 161–162 | 166–168 [54] |
| **7l** | $3\text{-}CH_3–C_6H_4$ | 35 | 90 | 172–174 | 176–177 [55] |
| **7m** | $4\text{-}CH_3–C_6H_4$ | 35 | 93 | 225–227 | 221–223 [50] |
| **7n** | 2-Furyl | 30 | 83 | 201–202 | 204–205 [55] |
| **7p** | 2-Thienyl | 35 | 83 | 211–214 | 208–209 [50] |
| **7o** | 3-Pyridyl | 35 | 86 | 222–225 | 226–228 [54] |

[a] Isolated yields

[b] Melting points were not corrected

## Catalyst recovery and reuse

The recovery and reusability of the catalyst are very important for commercial and industrial applications as well as green process considerations. Thus, the recovery and reusability of MNPs-AQ were investigated in the sequential reaction of benzaldehdye (1 mmol) with other reactants and MNPs-AQ (30 mg) as catalyst in refluxing $H_2O$/EtOH (1:1) for 30 min. After completion of the reaction, the resulting solidified mixture was diluted with hot EtOH (15 mL). Then, the catalyst was easily separated using an external magnet, washed with hot EtOH, dried under vacuum, and reused in a subsequent reaction. Nearly quantitative recovery of catalyst (up to 97%) could be obtained from each run. As seen in Fig. 7, the recycled catalyst could be reused five times without any additional treatment or appreciable reduction in catalytic activity. The recovered catalyst after five runs had no obvious change in structure, as shown by comparison of the FT-IR spectra to that of fresh catalyst (Fig. 8). The consistent structure and activity of recovered and reused MNPs-AQ catalyst indicate that the reused MNPs-AQ also shows excellent performance for the synthesis of 1,4-dihydropyridines.

## Experimental

All chemicals were purchased from Merck or Acros chemical companies and used without further purification. Melting points were measured by using capillary tubes on an electro thermal digital apparatus and are uncorrected. Known products were identified by comparison of

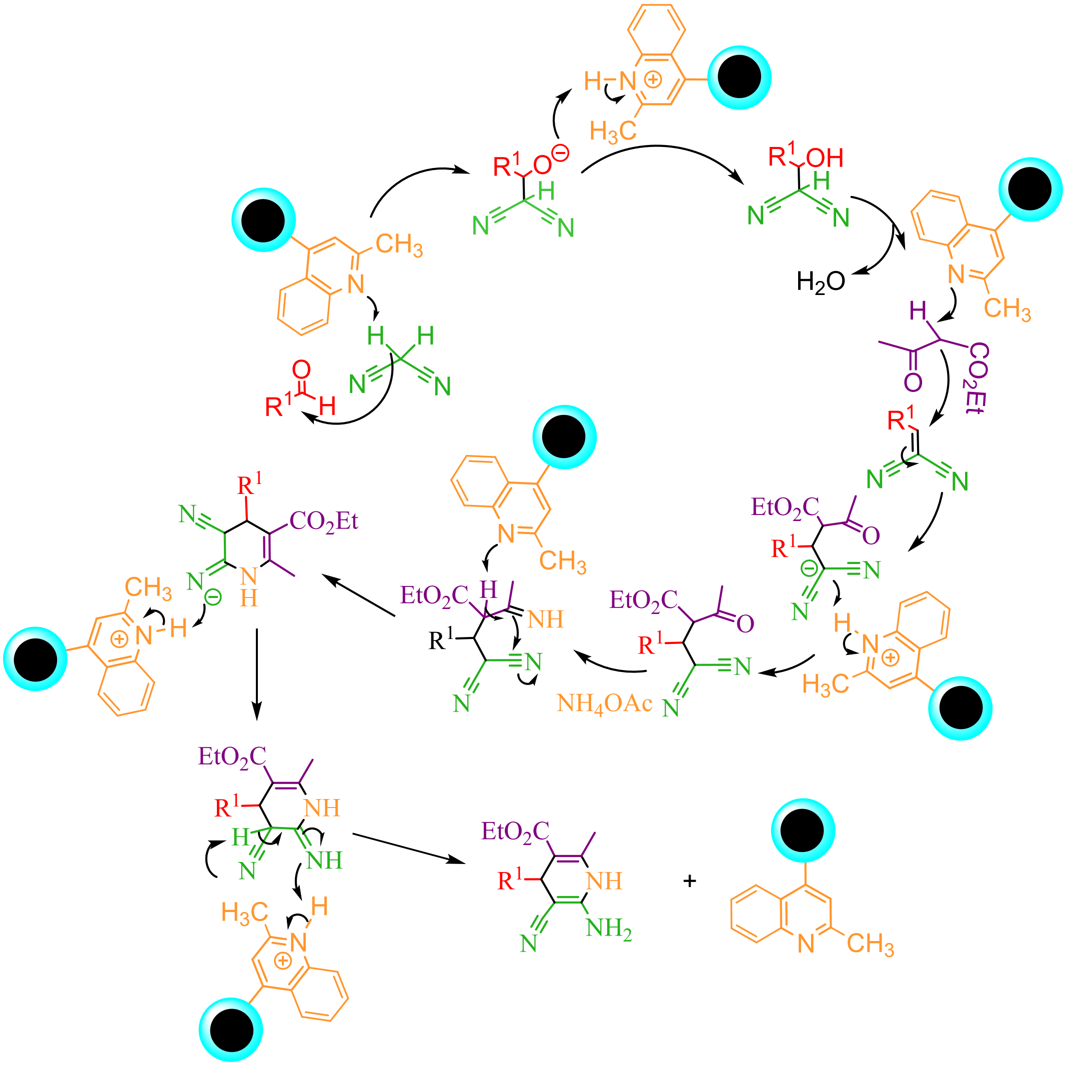

Scheme 3 The proposed mechanism for 1,4-dihydropyridine synthesis using MNPs-AQ catalyst

**Table 3** Comparison of MNPs-AQ with some other catalysts described in the literature for the synthesis of polyhydroquinolines

| Entry | Catalyst | Condition | Time (min) | Yield (%)[a] | References |
|---|---|---|---|---|---|
| 1 | [hmim]$BF_4$ | Solvent-free, 90 °C | 10 | 95 | [21] |
| 2 | L-proline | EtOH, rt | 120 | 85 | [12] |
| 3 | $I_2$ | Solvent-free, rt | 90 | 93 | [17] |
| 4 | CAN | Solvent-free, rt | 60 | 92 | [16] |
| 5 | $Yb(OTf)_3$ | EtOH, rt | 300 | 90 | [19] |
| 6 | MNPs@GSA | EtOH, reflux | 240 | 90 | [56] |
| 7 | $Hf(NPf_2)_4$ | $C_{10}F_{18}$, 60 °C | 180 | 95 | [57] |
| 8 | MNPs-AQ | EtOH:$H_2O$, reflux | 30 | 96 | Present work |

Reaction conditions: benzaldehyde (1 mmol), ethylacetoacetate (1 mmol), dimedone (1 mmol), ammonium acetate (1.2 mmol)

[a] Isolated yields

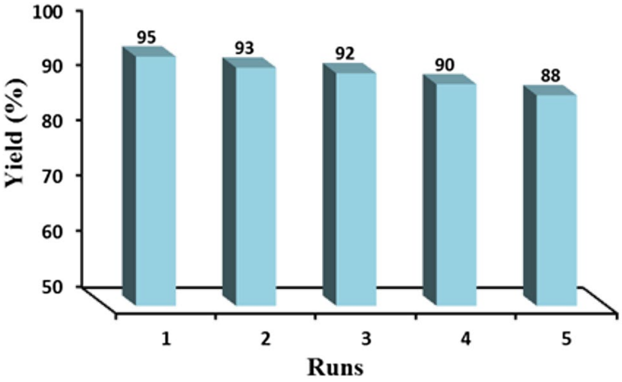

**Fig. 7** Recyclability of MNPs-AQ in the preparation of 1,4-dihydropyridines

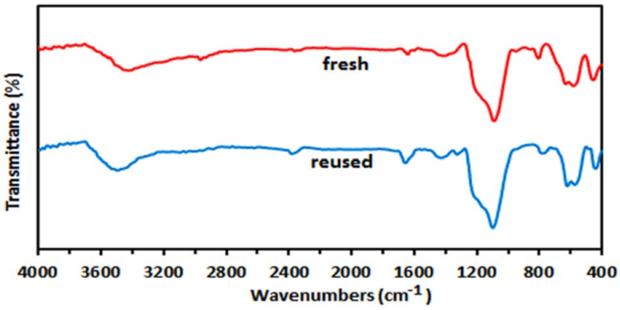

**Fig. 8** FT-IR spectra of the fresh catalyst and the five times reused catalyst

their spectral data and melting points with those reported in the literature. Thin-layer chromatography (TLC) was performed on UV active aluminum backed plates of silica gel (TLC Silica gel 60 F254). $^1$H and $^{13}$C NMR spectra were recorded on a Bruker Avance 300 MHz spectrometer at 300 MHz and 75 MHz, respectively. Coupling constants, J, were reported in hertz unit (Hz). IR spectra were recorded on a Unicom Galaxy Series FT-IR 5030 spectrophotometer using KBr pellets and are expressed in cm$^{-1}$. Elemental analyses were performed by Vario EL equipment at Arak University. X-ray diffraction (XRD) was performed on Philips XPert (Cu–K$_\alpha$ radiation, $\lambda = 0.15405$ nm) over the range $2\theta = 20°–80°$ using 0.04° as the step length. Thermalgravimetric analysis (TGA) and differential thermal gravimetric (DTG) data for MNPs-AQ were recorded on a Mettler TA4000 System under an $N_2$ atmosphere at a heating rate of 10 °C min$^{-1}$. The scanning electron microscope measurement was carried out on a Hitachi S-4700 field emission scanning electron microscope (FE-SEM).

### Preparation of the magnetic $Fe_3O_4$ nanoparticles

$Fe_3O_4$-MNPs were prepared using simple chemical co-precipitation described in the literature [44]. Briefly, $FeCl_2{\cdot}4H_2O$ (0.9941 g, 5 mmol) and $FeCl_3{\cdot}6H_2O$ (2.729 g, 10 mmol) were dissolved in 100 mL of deionized water in a three-necked round bottomed flask (250 mL). The mixture was heated under $N_2$ at 80 °C for 1 h, and then 10 mL of concentrated ammonia (25%) were added quickly. The solution was stirred under $N_2$ for another 1 h and then cooled to room temperature. The black precipitate formed was isolated by magnetic decantation, exhaustively washed with double-distilled water until neutrality, and further washed twice with ethanol and dried at 60 °C under vacuum.

### Synthesis of silica-coated MNPs ($Fe_3O_4@SiO_2$ MNPs)

The $Fe_3O_4@SiO_2$ core–shell nanoparticles were prepared according to the Stober method [45]. The details are as follows: Magnetic nanoparticles MNPs (1.0 g) were homogeneously dispersed by ultrasonic vibration in a mixture of 40 mL of ethanol, 6 mL of deionised water, and 1.5 mL of 25 wt% concentrated aqueous ammonia solution, followed by the addition of 1.4 mL of tetraethylorthosilicate (TEOS). After stirring for 12 h at room temperature under an $N_2$ atmosphere, the black precipitate ($Fe_3O_4@SiO_2$) was collected from the solution using a magnet, and then washed several times with water and ethanol and dried at 25 °C under vacuum.

### Synthesis of 3-chloropropyl-functionalized silica-coated magnetite nanoparticles ($Fe_3O_4@SiO_2$-PrCl MNPs)

In a typical procedure, 1.0 g of $Fe_3O_4@SiO_2$ MNPs were dispersed in 50 mL of dry toluene using an ultrasonic bath to produce a uniform suspension, to which 2.0 g of 3-chloropropyltrimethoxysilane (CPTMS) was added using a syringe. The resulting mixture was stirred for 24 h at 60 °C under an $N_2$ atmosphere. Finally, the chloropropyl-functionalized solid $Fe_3O_4@SiO_2$-PrCl MNPs were separated using a magnet, washed with toluene, and dried under vacuum.

### 4-Aminoquinaldine grafted on silica-coated magnetic nanoparticles (MNPs-AQ)

In a 100 mL round-bottomed flask, MNPs-AQ nanoparticles (1.0 g) were dispersed in 50 mL toluene using an ultrasonic bath. 1.9 g 4-aminoquinaldine (12 mmol) and 1.7 g triethylamine (12 mmol) were added to the suspension. The reaction mixture was refluxed at 100 °C for 24 h. The $Fe_3O_4@SiO_2$-AQ MNPs were washed with hot toluene an ethanol, separated using a magnet, and dried under vacuum at 60 °C.

## General procedure for the synthesis of 1,4-dihydropyridine derivatives

Aldehyde (1 mmol), malononitrile (1 mmol), ethyl acetoacetate (1 mmol), ammonium acetate (1.2 mmol), and MNPs-AQ (3 mg) as catalyst were mixed and refluxed in $H_2O$/EtOH (1:1) for appropriate time. After completion of the reaction as followed by TLC, the resulting solidified mixture was diluted with hot EtOH (15 mL). Then, the catalyst was separated using an external magnet, the solvent was evaporated, and the product was recrystallized with EtOH, and dried in an oven at 80 °C (Table 2).

## General procedure for the synthesis of polyhydroquinoline derivatives

A mixture of dimedone (1 mmol), ethylacetoacetate (1 mmol), aldehyde (1 mmol), ammonium acetate (1.2 mmol), and MNPs-AQ (30 mg) as catalyst in 5 mL $H_2O$/EtOH were stirred for appropriate time in reflux condition. After completion of the reaction as followed by TLC, the resulting solidified mixture was diluted with hot EtOH (15 mL). Then, the catalyst was separated using an external magnet, the solvent was evaporated, and the product was recrystallized with EtOH, and dried in an oven at 80 °C (Table 2).

# Conclusion

In this work, the 4-aminoquinaldine-functionalized silica coated magnetic nanoparticles (MNPs-AQ) successfully have been prepared and used as heterogeneous basic hybrid organocatalyst for one-pot synthesis of substituted 1,4-dihydropyridine and polyhydroquinoline derivatives under green conditions. Moreover, the catalyst can be easily separated and recovered from the reaction system by a magnet, and can be reused for several times without significant miss of its activity. In addition, the method presents various advantages including high yields, operational simplicity, clean reaction conditions, and minimum pollution of the environment, which makes it an effective and attractive procedure for the synthesis of these hydropyridine derivatives.

**Acknowledgements** The authors gratefully acknowledge the financial support from the Research Council of Arak University (Grant No. 95/5330).

# References

1. G. Swarnalatha, G. Prasanthi, N. Sirisha, C.M. Chetty, Int. J. ChemTech Res. **3**, 75 (2011)
2. G.M. Reddy, M. Shiradkar, A.K. Chakravarthy, Curr. Org. Chem. **11**, 847 (2007)
3. M. Inouye, T. Mio, K. Sumino, Eur. J. Clin. Pharmacol. **56**, 35 (2000)
4. C.O. Wilson, J.M. Beale, J.H. Block, *Wilson, Gisvold's Textbook of Organic Medicinal and Pharmaceutical Chemistry* (Lippincott Williams & Wilkins, Baltimore, 2011)
5. J. Briede, D. Daija, M. Stivrina, G. Duburs, Cell Biochem. Funct. **17**, 89 (1999)
6. G.L. Bird, A.T. Prach, A.D. McMahon, J.A. Forrest, P.R. Mills, B.J. Danesh, J. Hepatol. **28**, 194 (1998)
7. S. Cihat, S. Rahime, Mini-Rev. Med. Chem. **6**, 747 (2006)
8. A. Hantzsch, Justus Liebigs Ann. Chem. **215**, 1 (1882)
9. C. Simon, T. Constantieux, J. Rodriguez, Eur. J. Org. Chem. **2004**, 4957 (2004)
10. J.P. Wan, Y. Liu, RSC Adv. **2**, 9763 (2012)
11. R. Surasani, D. Kalita, A.V.D. Rao, K. Yarbagi, K.B. Chandrasekhar, J. Fluor. Chem. **135**, 91–96 (2012)
12. A. Kumar, R.A. Maurya, Tetrahedron **63**(9), 1946–1952 (2007)
13. S.A. Kotharkar, R.R. Nagawade, D.B. Shinde, Ukr. Bioorg. Acta **1**, 3–5 (2006)
14. J. Safari, S.H. Banitaba, S.D. Khalili, J. Mol. Catal. A Chem. **335**, 46–50 (2011)
15. F.M. Tamaddon, S. Moradi, J. Mol. Catal. A Chem. **370**, 117–122 (2013)
16. S. Ko, C.-F. Yao, Tetrahedron **62**(31), 7293–7299 (2006)
17. S. Ko, M.N.V. Sastry, C. Lin, C.F. Yao, Tetrahedron Lett. **46**(34), 5771–5774 (2005)
18. J.D. Akbari, S.D. Tala, M.F. Dhaduk, H.S. Joshi, Arkivoc **xii**, 126–135 (2008)
19. L.M. Wang, J. Sheng, L. Zhang, J.W. Han, Z. Fan, H. Tian, C.T. Qian, Tetrahedron **61**(6), 1539–1543 (2005)
20. A.G. Sathicq, G.P. Romanelli, A. Ponzinibbio, G.T. Baronetti, H.J. Thomas, Lett. Org. Chem. **7**, 511 (2010)
21. S.-J. Ji, Z.-Q. Jiang, J. Lu, T.-P. Loh, Synlett **5**, 831–835 (2004)
22. M. Li, W.-S. Guo, L.-R. Wen, Y.-F. Li, H.-Z. Yang, J. Mol. Catal. A Chem. **258**(1–2), 133–138 (2006)
23. R. Sridhar, P.T. Perumal, Tetrahedron **61**(9), 2465–2470 (2005)
24. G. Sabitha, G.S.K.K. Reddy, C.S. Reddy, J.S. Yadav, Tetrahedron Lett. **44**(21), 4129–4131 (2003)
25. M. Lei, L. Ma, L. Hu, Synth. Commun. **41**(13), 1969–1976 (2011)
26. D. Bandyopadhyay, S. Maldonado, B.K. Banik, Molecules **17**, 2643–2662 (2012)
27. A. Debache, W. Ghalem, R. Boulcina, A. Belfaitah, S. Rhouati, B. Carboni, Tetrahedron Lett. **50**(37), 5248–5250 (2009)
28. D.S. Rekunge, C.K. Khatri, G.U. Chaturbhuj, Tetrahedron Lett. **58**(12), 1240–1244 (2017)
29. M.A. Bodaghifard, M. Hamidinasab, N. Ahadi, Curr. Org. Chem. **22**(3), 234–267 (2018)
30. L. Han, S.W. Park, D.W. Park, Energ. Environ. Sci. **2**, 1286 (2009)
31. L. Han, H.J. Choi, S.J. Choi, B. Liu, D.W. Park, Green Chem. **13**, 1023 (2011)
32. B. Rác, A. Molnar, P. Forgo, M. Mohai, I. Bertóti, J. Mol. Catal. A Chem. **244**, 46 (2006)
33. M.A. Nasseri, M. Sadeghzadeh, J. Chem. Sci. **125**, 537 (2013)
34. V. Polshettiwar, R. Luque, A. Fihri, H. Zhu, M. Bouhrara, J.M. Basset, Chem. Rev. **111**, 3036 (2011)
35. S. Shylesh, V. Schünemann, W.R. Thiel, Angew. Chem. Int. Ed. **49**, 3428 (2010)
36. A. Farrokhi, K. Ghodrati, I. Yavari, Catal. Commun. **63**, 41 (2015)
37. J. Safari, Z. Abedi-Jazini, Z. Zarnegar, M. Sadeghi, J. Nanopart. Res. **17**, 1 (2015)
38. S. Rostamnia, M. Amini, J. Nanopart. Res. **16**, 1 (2014)
39. Y. Leng, K. Sato, Y. Shi, J.G. Li, T. Ishigaki, T. Yoshida, H. Kamiya, J. Phys. Chem. C **113**, 16681 (2009)

40. A.L. Morel, S.I. Nikitenko, K. Gionnet, A. Wattiaux, J. Lai-Kee-Him, C. Labrugere, B. Chevalier, G. Deleris, C. Petibois, A. Brisson, ACS Nano **2**, 847 (2008)
41. M.A. Bodaghifard, A. Mobinikhaledi, S. Asadbegi, Appl. Organomet. Chem. **31**, e3557 (2017). https://doi.org/10.1002/aoc.3557
42. M.A. Bodaghifard, S. Asadbegi, Z. Bahrami, J. Iran. Chem. Soc. **14**, 365–376 (2017)
43. S. Asadbegi, M.A. Bodaghifard, A. Mobinikhaledi, Res. Chem. Intermed. (2017). https://doi.org/10.1007/s11164-017-3200-4
44. K. Can, M. Ozmen, M. Ersoz, Colloids Surf B Biointerfaces **71**(1), 154–159 (2009)
45. W. Stöber, A. Fink, E. Bohn, J. Colloid Interface Sci. **26**, 62 (1968)
46. M.K. Marchewka, Mater. Sci. Eng. B **95**(3), 214–221 (2002)
47. G. Feng, D. Hu, L. Yang, Y. Cui, X.-A. Cui, H. Li, Sep. Purif. Technol. **74**(2), 253–260 (2010)
48. J. Giri, S.G. Thakurta, J. Bellare, A.K. Nigam, D. Bahadur, J. Magn. Magn. Mater. **293**(1), 62–68 (2005)
49. K. Petcharoen, A. Sirivat, Mat. Sci. Eng. B **177**, 421 (2012)
50. J. Safaei-Ghomi, R. Teymuri, H. Shahbazi-Alavi, A. Ziarati, Chin. Chem. Lett. **24**, 921 (2013)
51. J. Marco-Contelles, R. León, C. de Los Ríos, A. Guglietta, J. Terencio, M.G. López, A.G. García, M. Villarroya, J. Med. Chem. **49**, 7607 (2006)
52. J. Marco-Contelles, R. León, C. de Los Ríos, A. Samadi, M. Bartolini, V. Andrisano, O. Huertas, X. Barril, F.J. Luque, M.I. Rodríguez-Franco, B. López, M.G. López, A.G. García, M. do Carmo Carreiras, M. Villarroya, J. Med. Chem. **52**, 2724 (2009)
53. X. He, Y. Shang, Z. Yu, M. Fang, Y. Zhou, G. Han, F. Wu, J. Org. Chem. **79**, 8882 (2014)
54. R. León, C. de Los Ríos, J. Marco-Contelles, M.G. López, A.G. García, M. Villarroya, Eur. J. Med. Chem. **43**, 668 (2008)
55. A.M. Zonouz, D. Moghani, Synth. Commun. **41**, 2152 (2011)
56. M. Hajjami, B. Tahmasbi, RSC Adv. **5**, 59194 (2015)
57. M. Hong, C. Cai, W.B. Yi, J. Fluor. Chem. **131**(1), 111 (2010)